Design, Fabrication, and Performance Test of a Hovering-Based Flapping-Wing Micro Air Vehicle Capable of Sustained and Controlled Flight

Quoc-Viet Nguyen *, Woei Leong Chan, and Marco Debiasi
National University of Singapore

ABSTRACT

We present our insect-based hovering Flapping-Wing Micro Air Vehicle (FW-MAV) capable of sustained flight and control. The proposed design combines two fixed wings and two flapping wings to take advantage of the double clap-and-ling effects at the end of each half-stroke during one flapping cycle for high thrust production, and utilizes the fixed wings as the stabilizing surfaces and lift enhancement mechanism in forward flight. The FW-MAV has a wing span of 22 cm from wing tip-to-wing tip, weighs about 14.6 grams with onboard integration of radio control system including a radio receiver, an electronic speed control (ESC) for brushless motor, two servos for attitude flight controls of pitch and yaw, and a single cell lithium polymer (LiPo) battery (3.7 V). Moreover, passive wing rotation is utilized to simplify the design. Powered by the single cell LiPo battery, the FW-MAV can produce enough vertical thrust of 14.76 grams for lift-off at 10 Hz, and flap at maximum frequency of 12.4 Hz with average vertical thrust of about 24 grams. Experimental results show that the effect of wing clap significantly enhances thrust generation of about 44.82% when compared to the case without clap-and-fling effect, and the thrust-to-power ratio of the FW-MAV is about 3.93. Finally, free flight tests in terms of vertical take-off, hovering, and manual attitude control flight have been conducted to verify the flight performance of the insect-inspired FW-MAV. Onboard equipped with a 70 mAh LiPo battery, the FW-MAV can demonstrate a sustained and controlled flight of about three minutes.

http://www.imavs.org/

1 INTRODUCTION

NOWADAYS flapping-wing micro air vehicles (FW-MAVs) become more and more attractive flying model to many research scientists around the world since they are well-known for effectively flight performance by employing many unsteady aerodynamic mechanisms in a low range of Reynolds number, which is usually less than 10,000 [1], and agile maneuverability compared to their counter parts of fixed wing and rotary wing for indoor operation. Based on natural inspiration of bird flight and insect flight, man-made FW-MAVs have been split into two main categories: bird-inspired FW-MAVs and insect-inspired FW-MAVs. They both fly by flapping wings, but fundamentally differ from each other in many ways [2] in terms of design of wing kinematics and control mechanisms. Most of bird-inspired FW-MAVs known as ornithopter need an initial launching speed while flapping their wings to produce propulsion and lift to push them forward and to keep them aloft in air. Thus, they cannot take off vertically or hover. In contrast, one of the ultimate goals of insect-inspired FW-MAVs is hovering capability. For flight, an insect-inspired FW-MAV should flap its wings in a nearly horizontal plane [3] with a large flapping stroke angle and wing pitch to produce sufficient vertical thrust even without forward velocity, allowing them to fly at low forward speed or even hovering without stalling. The hover capability and potential high flight efficiency are the two key factors that FW-MAVs still draw researchers' attention. However, we might acquire an efficient FW-MAV only if we can properly mimic principles of nature's flyers such as birds and insects.

Recently, countless FW-MAVs have been developed and flown by both academia and industry, only a few FW-MAVs are able to demonstrate free hovering flight [4-12]. Perhaps it is due to the difficulty to cope with the inherent instability of the hovering-based flapping-wing platforms [13]. In 2009, the Nano Hummingbird [4] of AerovironmentTM (AV) became the only FW-MAV that met all of the Phase II technical milestone set out by DARPA [14]. Recently, TechJect [5] and Festo [6] have also announced their dragon-like four-winged FW-MAVs capable of hovering in 2012. Apart from the industries, the academia has also brought forth a few notable platforms [7-9] capable of hovering with onboard control system.

In this paper, we describe a hybrid insect-inspired design between flapping wing and fixed wing, and fabrication of a FW-MAV capable of vertical take-off and hovering. The FW-MAV shown in Figure 1 has a wing span of 22 cm from wing tip-to-wing tip, weighs less than 20 grams, and mimics some desirable features of insect flight such as large wing stroke angle, wing pitch angle, and clap-and-fling mechanism for high thrust production. Keeping in mind of natural inspiration of insect flight, we designed a gearbox mimicking an insect thorax by using four-bar linkages, in which clap-and-fling effects can be created at the end each half stroke: upstroke where the two flapping wings clap together at dorsal side (dorsal wing clap), and downstroke where the two flapping wings clap on the two fixed wings placed at the ventral side

*Email address: tslnqv@nus.edu.sg

http://www.imavs.org/

(ventral wing clap) of the FW-MAV. As shown in Figure 1, four wings are arranged around the fuselage, but only two wings flap, the other two wings are fixed. Thus, the platform is a hybrid between flapping wing and fixed wing. The fixed wings play main roles of creating clap-and-fling effect at ventral side for vertical thrust enhancement, stability, and lift enhancement for forward flight mode. In addition, passive wing pitch is incorporated into the FW-MAV by means of an initial slack angle implemented on the wing, and cylindrical hinges placed at the wing root. For stability and control, we still use the bird-like tail and control surface. Attitude control flight of pitch and yaw are performed by control surfaces (elevator and rudder) actuated by two servos. Finally, force measurement and free flight test allow us to characterize the performance of the FW-MAV in terms of vertical thrust production, dynamic flight stability, and control effectiveness; the FW-MAV can vertically take off at flapping frequency of 10 Hz, and carry a maximum payload of 9 gram at maximum flapping frequency of 12.4 Hz. Hovering flight can be easily achieved by control surface (elevator).

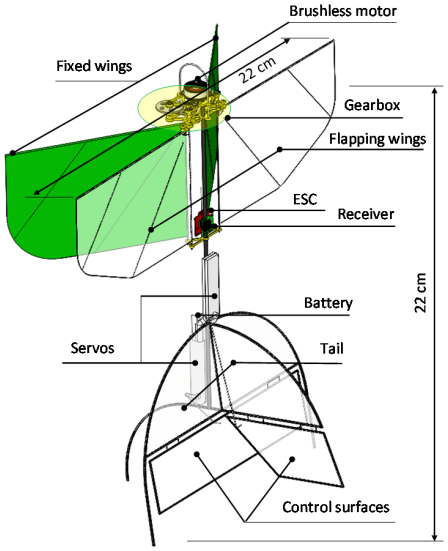

Figure 1: Three-dimensional SolidWorks model of the FW-MAV.

2 BIOMIMETIC DESIGN OF THE FW-MAV

With the inspirations from natural flyers, the design principle of the FW-MAV is to mimic some novel features of insect and hummingbird flights which can enable the FW-MAV to take off vertically and hover in air. Therefore, the flapping wings need to be configured in such a way that they provide enough vertical thrust for hovering flight.

2.1 Flapping mechanism

The foremost and most important thing we have to consider is the flapping mechanism used to drive the wings. For that purpose, we looked at an insect's wing joint system as shown in Figure 2, and mimicked it by using four-bar linkages (crank-rocker mechanism). This mechanism is simple and has one degree of freedom; each bar connects to two other bars by cylindrical joints as shown in Figure 3.

In order to drive the four-bar mechanisms, we use a gear system in which input links/cranks are fixed to the reduction gears (Figure 3). Thus, the rotary motion of the motor is directly transformed into the rotary motion of the input links. Sequentially, the four-bar mechanisms transform the rotary motion of the input link into the reciprocating motion of the output links/rockers where the wings are attached. In this design, we choose a flapping stroke angle of 130^o inspired from insect flight [1], and reduction gear ratio of 1 to 16 to utilize the maximal motor power at the half maximal speed. Figure 4 shown the position angle of the output link from the position analysis of the four-bar linkage under no load condition [15]. The mean flapping stroke angle is intentionally shifted to the dorsal side in order to create a clap-and-fling effect at the end of upstroke where the two flapping wings clap together. For accommodation for the flapping mechanism, we assembled a gearbox, Figure 5, in which we used 1 mm high gloss carbon fiber sheet to fabricate all the gearbox housing and links by mean of milling computer numerical control (CNC) machine (M300S CE, Woosung E&I Co. Ltd, Korea). The details of fabrication process can be found in the reference [9].

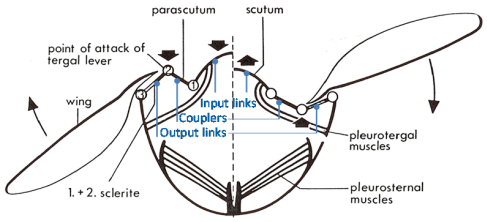

Figure 2: Wing joint system of an insect adapted from [16].

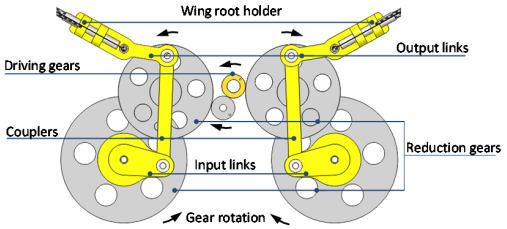

Figure 3: Gears and four-bar linkages mimicking insect's thorax.

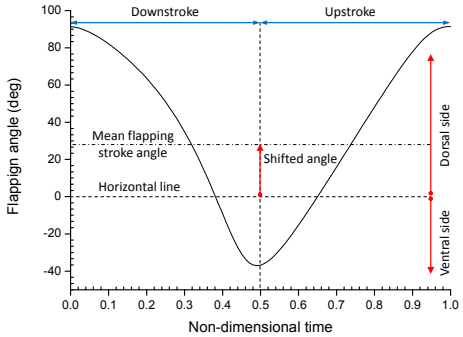

Figure 4: Position of flapping stroke angle of the output link.

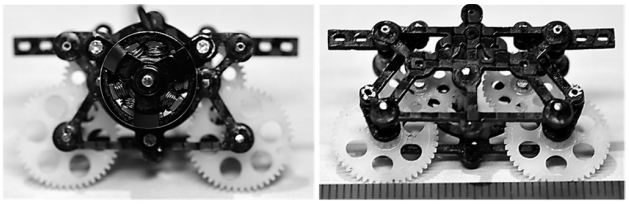

Figure 5: Full assembly of the gearbox (one brushless motor, two pinions, two 36/12 teeth spur gears, two 48/12 teeth spur gears, two four-bar mechanisms, and housing frames).

2.2 Wing and wing pitch mechanism

The flapping wings should be flexible to produce high thrust [17], but stiff enough to sustain the dynamic wing loading during flapping, and as light as possible to reduce the undesirable effect of wing inertia at high flapping frequency. For this purpose, we use lightweight but high strength materials: thin carbon rod (0.8 mm for leading edge and 0.3 mm for wing supporting veins) and thin Mylar film (15 μm) for membrane. The supporting veins are intentionally not joined with wing leading edge (WLE) allowing the wing to easily deform for wing rotation about WLE while maintaining the wing shape for aerodynamic force generation during flapping motion. Figure 6 shows a fabricated wing with the area of 61 cm^2, and the weight of 0.7 gram. The implemented initial slack angle, θ, is for passive wing pitch/rotation.

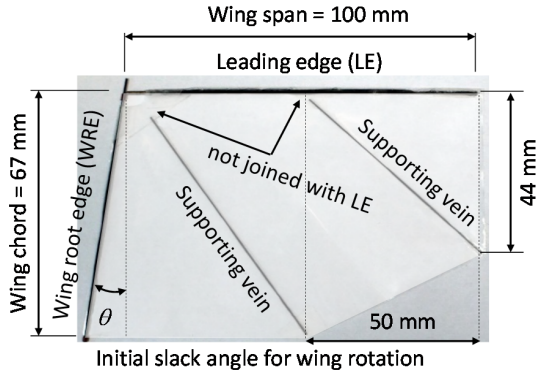

Figure 6: Wing made of carbon rods and Mylar film.

Insects fly by sweeping their wings at large flapping stroke angle and actively pronating and supinating their wings at the end of each half stroke. These active wing pronation and supination adjust the wings to a right angle of attack in order to capture vortices from the previous stroke for lift/thrust enhancement. Mimicking such an active wing pitch is a challenging part of design and requires a complex mechanism that may lead to weight penalty. Instead of that, a passive wing pitch mechanism induced by resultant aerodynamic forces and wing inertia is a simple and effective mechanism, and mostly used in current FW-MAVs. The feathering/rotational axis is located at the wing LE. When the wing flaps, resultant aerodynamic force on the wing makes it passively pitch about the feathering axis in clockwise (CW) or counter-clockwise (CCW) directions, as shown in Figure 7, resulting in vertical thrust production for both downstroke and upstroke. In order to prevent excessive wing pitch angle, we intentionally implement an initial slack angle, θ in Figure 6, on the wing to create an initial wing deformation when it is installed into the FW-MAV where the wing root edge (WRE) is perpendicularly aligned with the wing LE. Moreover, we utilize cylindrical hinges placed at the wing root, Figure 8, to allow free rotation of WLE and WRE for more effectively passive wing rotation. The maximum clock-wise (CW) and counter clock-wise (CCW) wing pitch angle, ψ in Figure 5, at wing tip is designed to be 30° for the downstroke and 30° for the upstroke, respectively, by implementing an initial wing slack angle of 5°; this angle was experimentally proved to be the best wing configuration for maximum lift production among various initial wing slack angles from 0° to 15°.

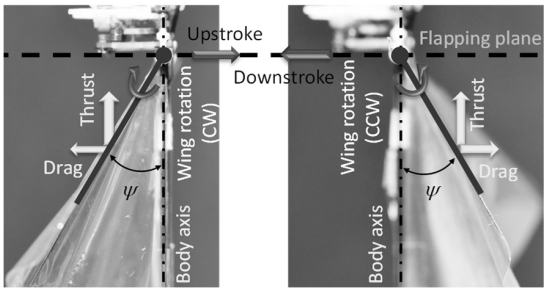

Figure 7: Passive wing pitch during downstroke and upstroke.

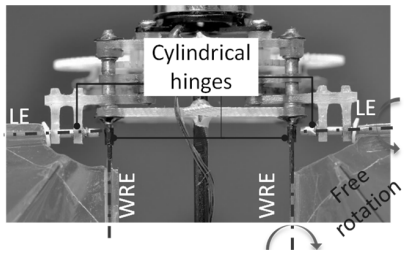

Figure 8: Cylindrical hinges at wing root for effectively wing rotation.

2.3 Wing clap-and-fling mechanism

Clap-and-fling mechanism proposed by Weis-Fogh [18], analyzed to confirm the existence and power of the concept by Lighthill [19], and quantitatively evaluated by Bennett [20] is one of the methods of insect flight along with the leading edge vortex method [21]. This mechanism allows the flapping wings to rapidly build and increase circulation due to absence of trailing edge vorticity [22], resulting in high lift/thrust production. Figure 9 describes the sequence of the clap-and-fling mechanism.

In this design, we mimic the insect wing clap-and-fling mechanism by designing a proper shape for the output links, where the flapping wings are attached, such that the wing claps can be created at the end of each half stroke: the end of upstroke where the two flapping wings clap together (dorsal wing clap), and the end of downstroke where the two flapping wings clap on the two fixed wings (ventral wing claps). Figure

http://www.imavs.org/

10 shows the flapping angle and implementation of wing claps into the FW-MAV. The effect of the wing claps on vertical thrust production was experimentally investigation in the section 3. Figure 11 indicates the wing claps captured by a high speed camera.

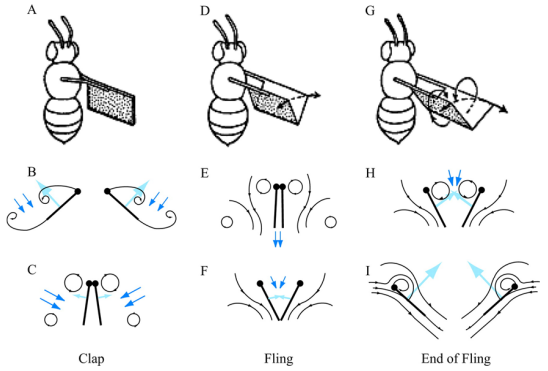

Figure 9: Clap-and-Fling mechanism proposed by Weis-Fogh and modern view adapted by SP. Sane [19].

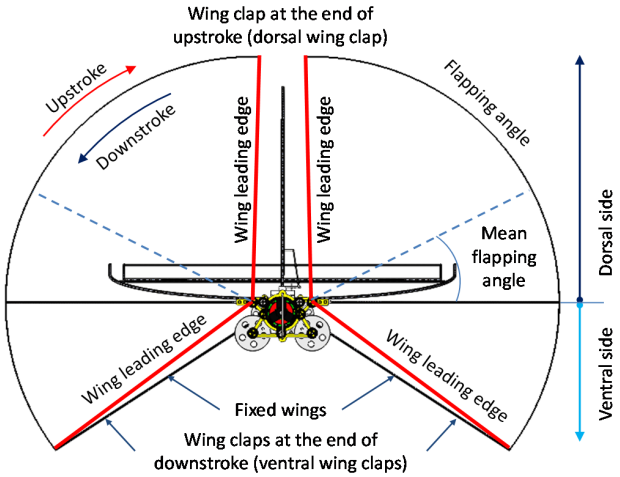

Figure 10: Top view: flapping stroke angle and wing claps at dorsal side and ventral side of the FW-MAV.

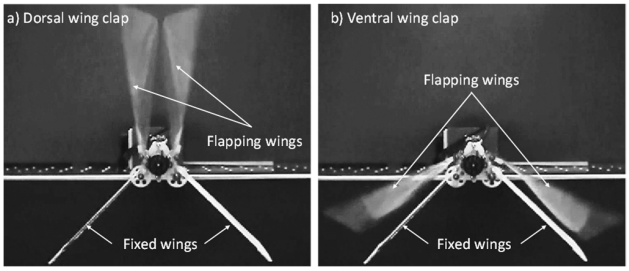

Figure 11: Wing claps at dorsal and ventral sides captured by a high speed camera.

2.4 *Control mechanisms and stability*

We use bird-like tail for stability and the conventional control surfaces as those in an airplane to simplify the design and perform attitude control of pitch and yaw for the FW-MAV. Figure 12 shows the control mechanism integrated on our present FW-MAV; the two control surfaces which are elevator and rudder are tilted by two servos. The elevator can be tilted up and down to create a pitching moment to rotate the FW-MAV about the Y-axis in CCW or CW direction, respectively. Similarly, the rudder can be tilted left and right to create a yawing moment to rotate the FW-MAV about the Z-axis. The two degrees of control allow us to effectively control the FW-MAV. Hovering and forward flight are performed by the elevator, and turning flight is performed by the rudder.

For stability of the FW-MAV, we implement inherent stability by using stabilizing surfaces which consist of the two fixed wings and tail as shown in Figure 1. By placing a proper location of center of gravity (CG), the FW-MAV can maintain good dynamic flight stability during free flight test performed in the section 4. Comprehensive stability analysis is not consider in this work.

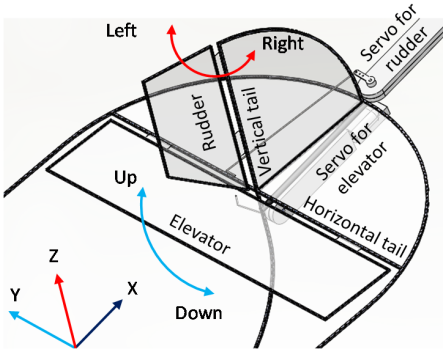

Figure 12: Tail and control mechanism.

2.5 *Electronic system integration*

The success of fabricating a controllable FW-MAV is somewhat determined by the availability of tiny size remote control components. Currently, the components used in the FW-MAV are all off-the-shelf. The receiver is the DelTang Rx31d compatible to Spektrum DSM2 protocol, weighs only 0.24 g, and it is among the smallest receiver for servo system available in the market. For motor, it is known that brushless motors provide higher efficiency at high speed operation compared to brushed motors. However, a brushless motor need an electronic speed controller (ESC) to operate. One might consider that as an added weight, but we manage to find a 0.3 g ESC (HK030, HobbyKing.com) for the 3.1 g brushless motor (AP-03, kv = 7000, HobbyKing.com) which we are using in our FW-MAV. For control purpose, we use the 0.8 g Toki BioMetal servos (Smart Servo RC-1, positive PWM signal of 1.5ms ± 0.5ms in every 20ms, www.toki.co.jp). Figure 13 and Figure 14 show the wiring diagram for the electronic system integration, and implementation of the electronic system on the fuselage, respectively. Figure 15 shows a complete assembly of the FW-MAV weighing 14.6 g whose detailed breakdown is shown in Figure 16 and parameters is listed in Table 1.

http://www.imavs.org/

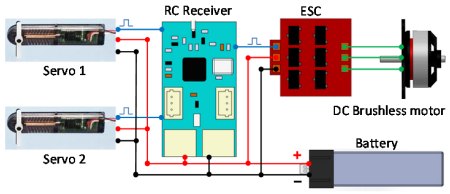

Figure 13: Wiring diagram for electronic components.

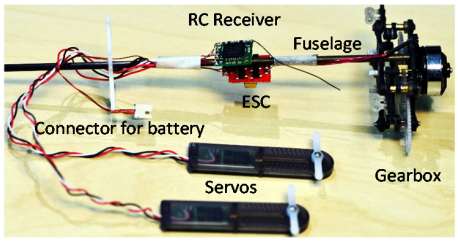

Figure 14: Electronic system integrated on the FW-MAV.

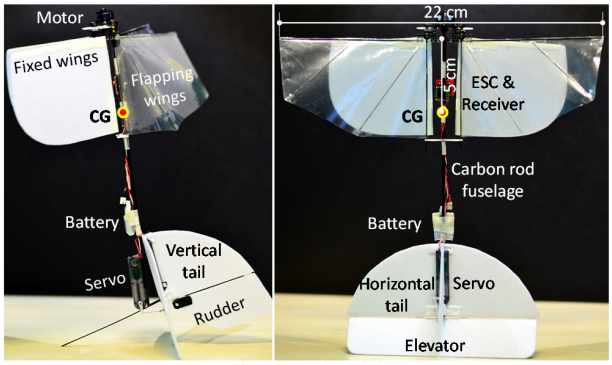

Figure 15: Full assembly of the FW-MAV.

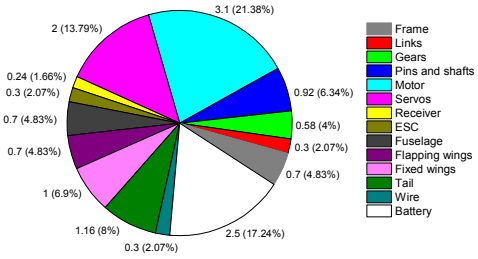

Figure 16: Weight breakdown of the FW-MAV in gram and percentage.

Parameters	Value
Mass	14.6 grams
Wing flapping frequency	10 Hz – 12.4 Hz
Take-off flapping frequency	10 Hz
Flapping stroke angle	125°
Wing length	10 cm
Wing span (wing tip-to-wing tip)	22 cm
Wing area (one wing)	61 cm^2
Wing loading	0.12 $gram/cm^2$
Wing aspect ratio	1.64
Mean chord length	6.1 cm
Mean wing tip velocity at 12.4 Hz	5.41 m/s
Reynolds number [1] at 12.4 Hz	10921

Table 1: Parameters of the FW-MAV.

3 FORCE PRODUCTION AND POWER CONSUMPTION

3.1 Experimental set-up

The force measurement was conducted to characterize the performance of the FW-MAV at various flapping frequency. Figure 17 shows the experimental set-up for force and power consumption measurement; the FW-MAV excluding tail and control mechanism was vertically mounted on a test jig consisting of a 3-axis force/torque loadcell (ATI Titanium Nano 17, ATI Industrial Automation), and a fixture. The loadcell can simultaneously sense six force components (3 forces and 3 moments), but only vertical force is considered in this test. An external power supply (Tenma 72-8350) was used in order to constantly maintain the applied voltage of 3.7 V to the motor. High voltages were refrained from applying because they are not compatible with the onboard electronic system. In order to reduce data contamination due to vibration of the FW-MAV itself and supporting structure, the sensing surface of the load cell was placed at the CG of the FW-MAV (Figure 15), and thus allowing us to obtain repeatable force data. To eliminate the undesired high peaks due to the vibration of the FW-MAV and structure vibration, we filtered the measured raw data by a low pass filter with a cut-off frequency that was 2.5 times greater than the flapping frequency. Thus, the filtered data included the effect of clap-and-fling and wing rotation frequency which happen two times in a flapping cycle. For each frequency, we carried out five tests for force measurement. Then, we took the cycle-average value of 20 cycles for each test and the statistical mean value of five tests to represent the average force generated by the FW-MAV.

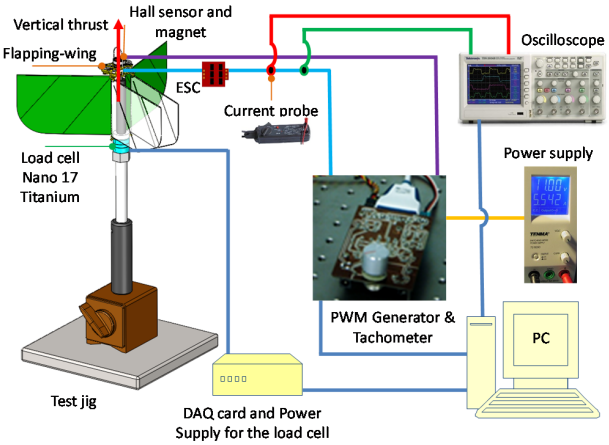

Figure 17: Experimental set-up for force and power consumption measurement.

To control flapping frequency of the FW-MAV, a Neodymium magnet is placed in a gear, where the input link is attached, and a Hall Effect switch is installed to pick up the magnetic signal from the magnet. Every time the magnet passes through the Hall Effect switch, an electrical pulse is generated and then transmitted to a tachometer circuit built in house, Figure 17. A micro-controller in the tachometer circuit

http://www.imavs.org/

http://www.imavs.org/

determines the flapping frequency and transmits the data to a computer via RS-232 port. The circuit also consists of a pulse width modulation (PWM) generator of which we can control the 1 ms to 2 ms pulse width by tuning the knob on the circuit, Figure 17. The PWM signal is transmitted to the electronic speed controller (ESC), and thus changes the motor speed, resulting in changing flapping frequency of the FW-MAV up to maximum value of 12.4 Hz.

Power consumption of the FW-MAV is calculated by voltage and current which were measured by an oscilloscope (TDS 2024B, Tektronix) and a current probe (CP-06 AC/DC, Kilter Electronic Institute) arranged as in Figure 17. The current probe sense the current flowing through a conductor and convert it to a voltage that can be viewed and measured on the oscilloscope. Channels 1 and 2 of the oscilloscope were used to read voltage applied to the motor, and voltage from the current probe, respectively. The voltage measured by the current probe was then converted into current by multiplying by the conversion factor indicated on the current probe.

3.2 Vertical thrust and effect of wing clap-and-fling

Force measurement was conducted for several flapping frequencies from 9 Hz to 12 Hz in which the FW-MAV produces enough thrust for take-off and flight. To investigate how the wing clap-and-fling affects vertical thrust generation, we conducted force measurement for three different flapping conditions: single wing only in which only one wing was installed into the flapping testing system, dorsal wing clap-and-fling in which two flapping wings clap together at the dorsal side, and dorsal & ventral wing clap-and-fling in which the two flapping wings clap together at the dorsal side (dorsal wing clap-and-fling) and clap on the two fixed wings at the ventral side (ventral wing clap-and-fling), respectively. The contributions of the wing clap-and-fling effects were examined by comparing the mean vertical thrusts produced by the FW-MAV for the three cases. Comprehensive investigation of this effect is out of this work scope, we leave it for future work.

The results shown in Figure 18 indicate the nearly linear relationship between flapping frequency and thrust in which the mean thrusts and standard deviations were statistically calculated from five measurements at each flapping frequency (9 Hz, 10 Hz, 11 Hz, and 12 Hz). Theoretically, the thrust is proportional to velocity or frequency square. Therefore, the nearly linear relationship obtained from the experiment can be explained by the induced velocity which reduces effective angle of attack; the induced velocity increases as the flapping frequency increases, resulting in reducing effective angle of attack. Thus, lift on the flapping wing is reduced.

At flapping frequency of 10 Hz the FW-MAV produces 14.76 grams thrust, which is slightly higher than its own weight of 14.6 grams, and starts to take off. At flapping frequencies of 11 Hz and 12 Hz, the FW-MAV can carry payloads of 3.3 grams and 7.2 grams, respectively, thus allowing us to implement a small camera onboard for the next version of the FW-MAV.

Wing clap-and-fling effects at dorsal and ventral sides were examined by comparing the two cases of dorsal wing clap-and-fling and single wing x 2 (which is calculated by multiplying the single wing case by 2), and the two cases of dorsal & ventral wing clap-and-fling and dorsal wing clap-and-fling, respectively. As shown in Figure 18, the wing clap-and-fling effect significantly increases the average vertical thrust. When compared to the case of single wing x 2, the dorsal wing clap-and-fling and dorsal & ventral wing clap-and-fling contribute to a thrust increase of 30.22% and 44.82%, respectively, at flapping frequency of 12 Hz. When compared to the case of dorsal wing clap-and-fling, the dorsal & ventral wing clap-and-fling produces a thrust increase of 1.73 grams (13.26% increase), 2.02 grams (12.68% increase), and 3.14 grams (16.83% increase) at frequencies of 10 Hz, 11 Hz, and 12 Hz, respectively. Therefore, it is worth to install the two fixed wings with weight of 1 gram to have higher thrust production.

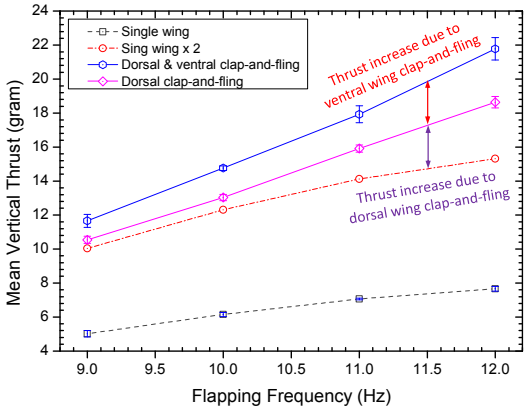

Figure 18: Mean vertical thrust and standard deviation for five measurements at each flapping frequency.

The measured thrusts indicates that the positive value dominates the thrust profile in both downstroke and upstroke. That means the passive wing rotation mechanism is properly implemented into the FW-MAV. The two peaks in the thrust profile/time-dependent thrust are due to the wing clap-and-fling effects at the end of each half flapping stroke: dorsal wing clap-and-fling and ventral wing clap-and-fling. The gaps between the time-dependent thrusts for the three cases of flapping condition at these two peaks indicate the wing clap-and-fling effects. As shown in Figures 19, 20, and 21 for three cases of flapping frequency (10 Hz, 11 Hz, and 12 Hz, respectively), the dorsal wing clap-and-fling creates a thrust increase at the higher peak (1st peak) when comparing the case of single wing x 2 to the cases of dorsal wing clap-and-fling and dorsal & ventral wing clap-and-fling, and the ventral wing clap-and-fling creates another thrust increase at the lower peak (2nd peak) when comparing the case of single wing x 2 and dorsal wing clap-and-fling to the case of dorsal & ventral wing clap-and-fling. We will further investigate these effects by the means of high speed cameras and smoke/He-bubble/PIV visualization in future to explain the high peak force in the time-dependent force profile. From the measured

http://www.imavs.org/

results, we obviously expected that the FW-MAV can demonstrate vertical take-off and free hovering flight.

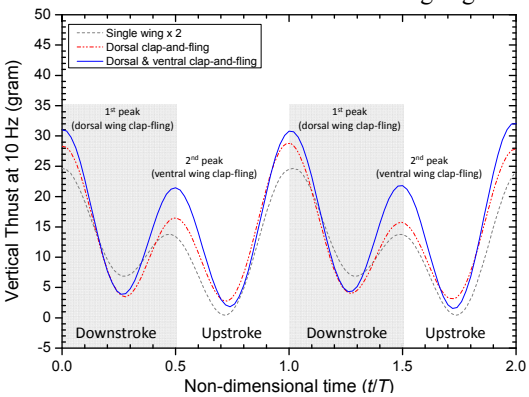

Figure 19: Time-dependent vertical thrust at 10 Hz.

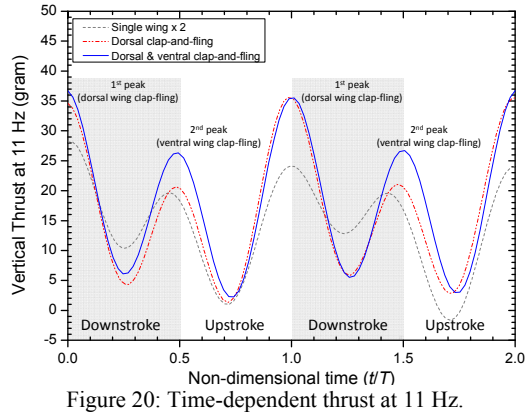

Figure 20: Time-dependent thrust at 11 Hz.

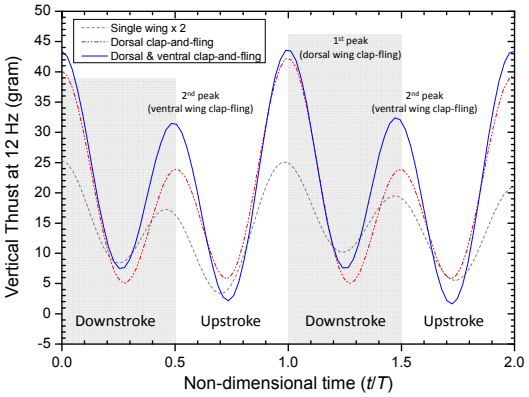

Figure 21: Time-dependent thrust at 12 Hz.

3.3 Power consumption

Power consumption was measured for two cases: gearbox only in which there was no wing installed into the FW-MAV, and full system (total power consumption) in which all wings were installed into the FW-MAV. Figure 22 shows the power consumption for the two cases from 9 Hz to 12 Hz. The power consumption due to the two flapping wings and wing inertia during flapping process was calculated by subtracting the power consumed by the gearbox only from the total power consumption. At flapping frequency of 9 Hz, 10 Hz, 11 Hz, and 12 Hz, the power consumed by the gearbox only or power loss due to the gearbox is 18.75%, 17.41%, 17.04%, and 16.67% of total power consumption, respectively. However, in this test the power consumed by the wing inertia is still not isolated; power measurement in vacuum condition will have to be conducted in future. From the measurement of power consumption and thrust, thrust-to-power ratio turns out to be 3.32, 3.46, 3.68, 3.93, respectively.

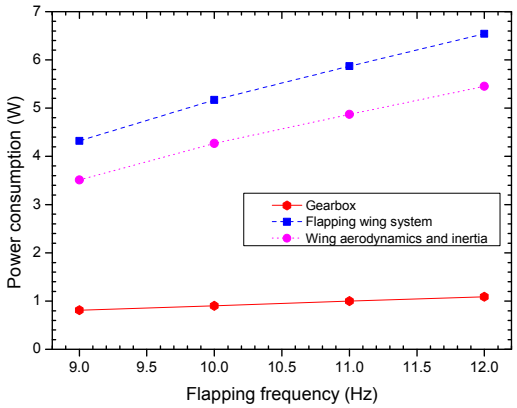

Figure 22: Power consumption of the FW-MAV at various flapping frequencies.

4 FREE FLIGHT TEST

Vertical take-off, sustained and controlled flight were conducted indoor with a radio transmitter (Spektrum DX7, DSM2) to demonstrate the flight abilities of the FW-MAV. The comprehensive study of stability and flight dynamics of the FW-MAV are not investigated in this work, we leave it to future work. The force measurement has proven that the FW-MAV produces sufficient thrust to lift off its own weight for flight. However, a visually real flight is much obviously to judge the force production of the FW-MAV. Thus, the take-off test was not only to verify the measured force but also to demonstrate the desired features of an insect-inspired FW-MAV: vertical take-off, and hovering. Moreover, the test was also to verify the inherent stability of the FW-MAV. Several take-off tests were conducted and captured by an ordinary camera, the captured were then extracted to build a composite image of take-off process. Figure 23 indicates the FW-MAV can demonstrate vertical take-off and then hovering.

In addition to the take-off test, free indoor flight test was also conducted to demonstrate and verify the sustained flight and control effectiveness, respectively. A simple mission was carried out as shown in Figure 24, which illustrates the flying sequence of the mission: take-off → hovering → attitude controlled flight → hovering → landing. Firstly, the FW-MAV vertically took off, and was tuned in hovering flight mode by using elevator. Transition flight from hover to forward flight/turning flight and vice versa could be achieved by both elevator and rudder. The mission lasting about one minute was successful accomplished. However, vertical

landing is still not achieved, the FW-MAV tends to be fallen down when it touches the ground. Thus, we will design a proper landing gear for the FW-MAV. Overall, our FW-MAV shows a good apparent performance and demonstrates a desirable feature of insect flight: hovering capability.

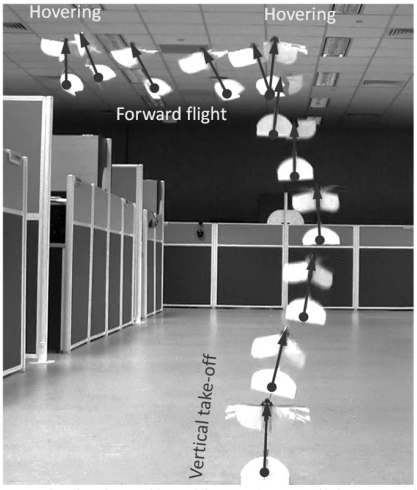

Figure 23: Vertical take-off and hovering, solid arrow denotes the body axis of the FW-MAV.

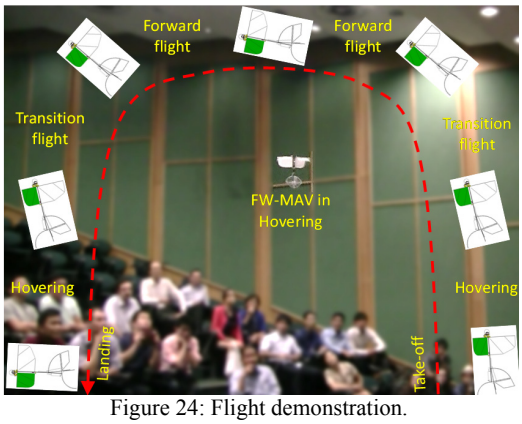

Figure 24: Flight demonstration.

5 CONCLUDING REMARKS

In summary, we presented a road map to achieve a hovering flapping-wing micro air vehicle mimicking principle of insect flight that involves translating a design concept into an actual flying flapping-wing prototype and then achieving the successful free flight with control authority. Our proposed hybrid design utilizes the clap-and-fling effects of insect flight for high thrust production that enable our 22 cm wing span hybrid insect-inspired FW-MAV to vertically take off and hover in air. Moreover, the measured vertical thrust of about 22 grams at applied voltage of 3.7 V and flapping frequency of 12 Hz indicates that the FW-MAV produces sufficient lift for hovering flight and payload carrying such as a system integration of a small camera for vision and a sensor for automatic control on the future versions of the FW-MAV. Future work will focus on further onboard system integration for better control abilities, improving the FW-MAV such as implementation of compliant mechanism for energetic cost reduction, optimum wing design for high lift production, and unsteady flow visualization such as leading vortex mechanism, vortex shedding, clap-and-fling effect, and the generation of a downward flow for further performance improvement.

ACKNOWLEDGMENT

Authors appreciate the financial support from Defence Research & Technology Office of Singapore (Programme No. PA 9011102539).

REFERENCES

[1] C. P. Ellington. The novel aerodynamics of insect flight: Applications to microair vehicles. *J. Exp. Biol*., 202: 3439–3448, 1999.
[2] W. Shyy, H. Aono, CK. Kang, and H. Liu. *An Introduction to Flapping Wing Aerodynamics*. Cambridge Aerospace Series, Cambridge University Press, 2013.
[3] F.O. Lehmann and S. Pick. The aerodynamic benefit of wing–wing interaction depends on stroke trajectory in flapping insect wings. *J. Exp. Biol*., 210: 1362–1377, 2007.
[4] Nano Hummingbird, available at http://www.avinc.com/nano
[5] The Robot Dragonfly, available at http://www.techject.com/
[6] BionicOpter–Inspired by dragonfly flight, available at http://www.festo.com/cms/en_corp/13165.htm
[7] P. Zdunich, D. Bilyk, M. MacMaster, D. Loewen, J. DeLaurier, R. Kornbluh, T. Low, S. Stanford, and D. Holeman. Development and testing of the mentor flapping-wing micro air vehicle. *J. Aircraft*, 44 (5): 1701–1711, 2007.
[8] http://www.delfly.nl/home.html
[9] Q.V. Nguyen, W.L. Chan, and M. Debiasi. Development of an insect-inspired flapping-wing micro air vehicle capable of vertical take-off and hovering. In *IEEE/RSJ Int. Conf. on Intelligent Robots and Systems*, Chicago, Illinois, Sept. 14–18, 2014. submitted for publication
[10] C. Richter, H. Lipson. Untethered hovering flapping flight of a 3D-printed mechanical insect. *Artificial Life*, 17: 73–86, 2011.
[11] F. van Breugel, W. Regan, and H. Lipson. From insects to machines: A passively stable, untethered flapping-hovering micro-air vehicle. *IEEE Robot. Autom. Mag*., 15 (4): 68–74, 2008.
[12] L. Ristroph, S. Childress. Stable hovering of a jellyfish-like flying machine. *J. R. Soc. Interface*, 11, 2014.
[13] Y.L. Zhang and M. Sun. Control for small-speed lateral flight in a model insect. *Bioinsp. Biomim.*, 6, 2011.
[14] "AV Achieves Technical Milestone: controlled hovering flight of NAV with two flapping wings," AeroVironment Press Release, June 30, 2009.
[15] D. B. Doman, C. P. Tang, and S. Regisford. Modeling interactions between flexible flapping wing spars, mechanisms, and drive motors. *J. Guidance, Control, and Dynamics*, 34(5): 1457-1473, 2011.
[16] G.J. Goldsworthy, and C.H. Wheeler. *Insect Flight*. Boca Raton, Florida: CRC Press, Inc., 1989.
[17] M. Vanella, T. Fitzgerald, S. Preidikman, E. Balaras, and B. Balachandran. Influence of flexibility on the aerodynamic performance of a hovering wing. *J. Exp. Biol*., 212: 95–105, 2009.
[18] T. Weis-Fogh. Unusual mechanisms for the generation of lift in flying animals. *Scient. Am*., 233: 80–87, 1975.
[19] M. Lighthill. On Weis-Fogh mechanism of lift generation. J. *Fluid Mechanics,* 60: 1–17, 1973.
[20] L. Bennett .Clap and fling aerodynamics - An experimental evaluation. *J. Exp. Biol*., 69: 261–273, 1977.
[21] C.P. Ellington, C. van den Berg, A.P. Willmott, and A.L.R. Thomas. Leadingedge vortices in insect flight. *Nature*, 384 (6610): 626–630, 1996.
[22] S.P. Sane. Steady or unsteady? Uncovering the aerodynamic mechanisms of insect flight. *J. Exp. Biol*., 214 (3): 349-351, 2011.

http://www.imavs.org/